remote sensing

MDPI

Article

Quantitative Assessment of Volcanic Thermal Activity from Space Using an Isolation Forest Machine Learning Algorithm

Claudia Corradino [1,*], Arianna Beatrice Malaguti [1], Micheal S. Ramsey [2] and Ciro Del Negro [1]

[1] Istituto Nazionale di Geofisica e Vulcanologia, Sezione di Catania, Osservatorio Etneo, 95125 Catania, Italy; arianna.malaguti@ingv.it (A.B.M.); ciro.delnegro@ingv.it (C.D.N.)
[2] Department of Geology and Environmental Science of Pittsburgh, University of Pittsburgh, Pittsburgh, PA 15260, USA; mramsey@pitt.edu
* Correspondence: claudia.corradino@ingv.it

Abstract: Understanding the dynamics of volcanic activity is crucial for volcano observatories in their efforts to forecast volcanic hazards. Satellite imager data hold promise in offering crucial insights into the thermal behavior of active volcanoes worldwide, facilitating the assessment of volcanic activity levels and identifying significant changes during periods of volcano unrest. The Moderate Resolution Imaging Spectroradiometer (MODIS) sensor, aboard NASA's Terra and Aqua satellites, provides invaluable data with high temporal and spectral resolution, enabling comprehensive thermal monitoring of eruptive activity. The accuracy of volcanic activity characterization depends on the quality of models used to relate the relationship between volcanic phenomena and target variables such as temperature. Under these circumstances, machine learning (ML) techniques such as decision trees can be employed to develop reliable models without necessarily offering any particular or explicit insights. Here, we present a ML approach for quantifying volcanic thermal activity levels in near real time using thermal infrared satellite data. We develop an unsupervised Isolation Forest machine learning algorithm, fully implemented in Google Colab using Google Earth Engine (GEE) which utilizes MODIS Land Surface Temperature (LST) data to automatically retrieve information on the thermal state of volcanoes. We evaluate the algorithm on various volcanoes worldwide characterized by different levels of volcanic activity.

Keywords: machine learning; volcano monitoring; thermal anomaly; thermal activity level; satellite remote sensing; MODIS LST

Citation: Corradino, C.; Malaguti, A.B.; Ramsey, M.S.; Del Negro, C. Quantitative Assessment of Volcanic Thermal Activity from Space Using an Isolation Forest Machine Learning Algorithm. *Remote Sens.* **2024**, *16*, 2001. https://doi.org/10.3390/rs16112001

Academic Editor: Gianluca Groppelli

Received: 25 April 2024
Revised: 27 May 2024
Accepted: 30 May 2024
Published: 1 June 2024

1. Introduction

Volcanic eruptions can generate a variety of products that contribute to thermal anomalies detected by satellite observations. These products include lava flows, pyroclastic flows, ash plumes/clouds, and volcanic gases, each exhibiting distinct thermal characteristics [1]. The cooling of lava flows following an eruption can result in decreasing sur-face temperatures over time, leading to identifiable thermal anomaly behavior [1]. Pyro-clastic flows, consisting of hot volcanic ash, gases, and fragmented rock, generate intense thermal signatures due to their high temperatures and rapid movement downslope [2]. Additionally, the presence of volcanic ash plumes/clouds in the atmosphere can alter the Earth's radiation balance, influencing surface temperatures and producing thermal anomalies near the vent [3]. Furthermore, volcanic gases, such as sulfur dioxide (SO_2) and carbon dioxide (CO_2), can contribute to thermal anomalies through their interactions with the atmosphere, affecting infrared radiation absorption and emission processes [4].

Nowadays, satellite remote sensing is widely employed for monitoring volcanic thermal activity globally [5–21]. Numerous volcanic hotspot monitoring satellite platforms have been developed for the near real-time monitoring of thermal anomalies, such as MODVOLC [22], HOTVOLC [23], FIRMS [24], MIROVA [25] and LAV@HAZARD [26]. In

particular, MIROVA and MODVOLC use images acquired from the Moderate Resolution Imaging Spectroradiometer (MODIS) aboard NASA's Terra and Aqua polar satellites, providing data four times per day with a spatial resolution from 250 to 1000 m. These platforms employ the combination of MidInfrared (MIR) and Thermal Infrared (TIR) bands to detect thermal anomalies at high temperatures, from about 600 K upwards. Thermal Infrared (TIR) remote sensing measurements of high-temperature volcanic features offer unique insights into the dynamic behavior of volcanic systems. The emission of thermal energy from volcanic systems plays a crucial role in monitoring volcanic activity. Detecting thermal anomalies within volcanic regions can indicate potential changes in volcanic systems. The emergence of intense hotspots commonly signifies that the magmatic system is breaching the surface, whereas subtle anomalies can indicate movement of magma or changes in the overlying hydrothermal system [27]. Extreme temperatures are typically observed during eruptive activity and in lava lakes, whereas lower temperatures are recorded in fumarole fields and during the formation or destruction of lava domes.

Rapid identification of thermal anomalies is essential for understanding the long-term dynamics and unrest of volcanic systems, typically complemented by other geophysical parameters, which can prompt alert level changes. Monitoring these changes relative to normal conditions is crucial for assessing volcanic hazards. The effectiveness of satellite-based techniques in detecting subtle to high thermal anomalies associated with volcanic activity has been widely demonstrated [28,29]. Moussallam et al. [28] utilized TIR data from MODIS to detect and monitor thermal emissions from volcanoes in the East African Rift. Similarly, Wright et al. [29] employed TIR remote sensing data to identify changes in surface temperature associated with volcanic unrest at Mount Erebus in Ant-arctica. Land Surface Temperature (LST) measurements, as derived from MODIS, have proven effective in capturing thermal changes [30], thereby highlighting surface warming processes [31–33].

From this perspective, various data processing methods have been proposed to detect thermal anomalies indicative of significant volcanic changes compared to "normal" conditions. A commonly adopted strategy relies on temporal information, where anomalies are identified as deviations from long-term average values [34–36]. Thus, the anomaly is the difference between what is happening and what is expected over a long-term average trend. However, uncertainties persist due to seasonal variations, local weather patterns, topography, and surface heterogeneity. The robust satellite technique (RST) has been widely employed for thermal anomaly detection, utilizing multi-temporal statistical methods for analyzing long-term satellite records under similar observation conditions (e.g., same month, same time of day, and same sensor data) [37–40]. RST considers the statistical characteristics of the historical data to discriminate possible abnormal behavior of current thermal signals. However, RST may struggle to eliminate short-term meteorological warming impacts. Hill et al. [41] proposed another approach based on modeling the signal under "normal" conditions and considering anomalies as portions of the signal that the model fails to reconstruct accurately, which has been used across various fields. This method fits the time series under normal conditions, minimizing reconstruction errors. Where anomalies are present, deviations from expected patterns trigger anomaly detection based on reconstruction statistics.

We adopt a comparable approach utilizing an unsupervised machine learning (ML) model for anomaly detection capable of finding structure in the MODIS Land Surface Temperature (LST) data and clustering the detections based on data similarity. The ML model reconstructs error time series to automatically retrieve significant changes without external bias and a priori choices. Data drive the anomaly detection process. Specifically, we employ an Isolation Forest (IF) machine learning algorithm, an unsupervised decision tree-based algorithm originally designed for outlier detection in tabular data. The Isolation Forest technique randomly splits sub-samples of the data according to attributes/features/columns, with rarer observations more likely to be isolated quickly, indicating outlier status, i.e., fewer splits are needed to isolate an outlier (create a partition in which only one point is present). Furthermore, we exploit the capability of the Isolation Forest algorithm to

recognize anomalies to distinguish the activity levels. We determine different activity levels based not only on intensity differences but also on the difficulty of isolating sample points belonging to the time series using the Isolation Forest technique. We establish a framework on Google Colaboratory, commonly referred to as Colab, designed to automate the processing of MODIS LST datasets. This framework enables the extraction of detected anomalies and various activity levels, thereby facilitating global monitoring of volcanic thermal activity.

2. Materials

Volcanoe Selection

We investigated six volcanoes located in different areas around the world (Figure 1) in order to account for heterogeneity in our dataset: Etna and Stromboli (Italy), Klyuchevskoy (Kamchatka, Russia), Lascar (Chile), Popocatépetl (Mexico), Fuego (Guatemala). These volcanoes were selected for their wide variety of eruptive styles and time recurrence of eruptions between 2000 and 2023. With the exception of Stromboli, these same volcanoes were also investigated by Ramsey et al. [42] using higher-spatial-resolution Advanced Spaceborne Thermal Emission and Reflection Radiometer (ASTER) data.

- Mt. Etna is a large basaltic composite volcano located on the east coast of Sicily (Italy). Although Etna is a prevalently effusive volcano, since 1986, there has been a clear increase in explosive eruptions of medium intensity from the summit craters, better known as paroxysmal events. These events are characterized by the development of several km high ash plumes and lava overflows from the crater rim [43].
- Klyuchevskoy is an active and relatively young volcano located in the northern part of the Central Kamchatka Depression (Russia). Its recent activity is characterized by the effusion of voluminous basaltic andesite lava flows, commonly associated with moderate to violent explosive activity [44].
- Lascar volcano is a composite active stratovolcano located in the Antofagasta Region of Chile. The activity of the Lascar volcano is characterized by the persistent fumarolic activity, occasional small steam explosions with phreatic characteristics, the formation of lava flows, and explosive events [45,46]. Dome building and collapse have also been observed [47].
- Popocatépetl is an andesitic stratovolcano that lies ∼60 km SE of Mexico City (Mexico). The ongoing eruptive activity of Popocatépetl volcano has been characterized by vulcanian explosions, ash-poor "exhalations" of volcanic gas, and periodic lava dome growth, subsidence, and explosive destruction [48].
- Volcán de Fuego (or Fuego) is the most active stratovolcano in Guatemala. Since 1999, Fuego has been in a new period of eruptive activity characterized by persistent activity consisting of slow lava effusion, discrete strombolian and ash-rich explosions, and occasional higher-intensity explosive paroxysmal eruptions [49,50].
- Stromboli is the north-easternmost island of the Aeolian archipelago (Italy). The activity consists of intermittent mild explosions [51]. The ordinary activity is periodically broken by the emission of lava flow and by two types of violent explosions known as "major explosions" and "paroxysms" [52].

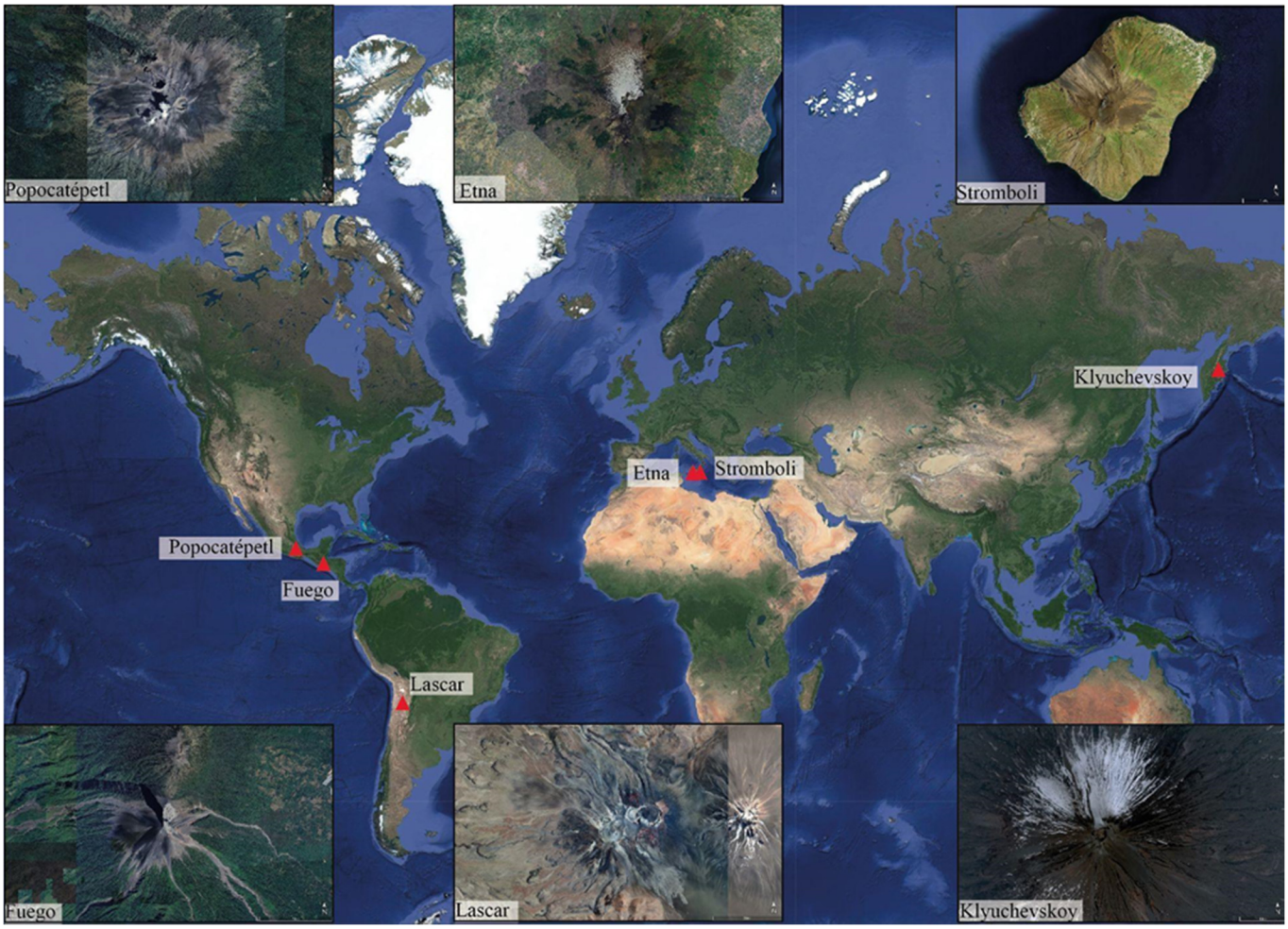

Figure 1. Overview and representative image of the volcanoes studied. All images were captured via Google Earth Pro [http://www.earth.google.com; accessed on 27 March 2024] and QGIS [https://qgis.org/it/site/; accessed on 27 March 2024].

3. Data

The satellite images and derived Land Surface Temperature (LST) data were acquired from the MODIS sensor onboard both the Terra and Aqua satellites. MODIS provides Medium Infrared (MIR) and Thermal Infrared (TIR) data at high temporal/low spatial resolution, allowing the identification and monitoring of volcanic thermal activity with data available 2–4 times per day at most volcanoes. The LST measurements obtained from MODIS offer valuable insights into surface temperature variations, which are essential for detecting and quantifying thermal anomalies associated with volcanic eruptions. We utilized data processing tools in Google Earth Engine (GEE) to access and analyze the MODIS LST data [53]. GEE is a cloud computing platform that makes it easy to access geospatial data for processing and visualizing, ideal for large-scale analysis of satellite observations. It is worth noting that this product is already masked for clouds, meaning that pixels containing clouds are removed. MODIS LST satellite images are pre-processed by selecting the ROI (Region of Interest) around the targeted volcano and by filtering out images from the collection that contain more than 50% of clouds in the selected ROI. For each volcano, the entire time series from 2000 to 2023 was analyzed.

4. Methods

We fit the LST time series under "normal" conditions using the Non-linear Least Squares (NLS) Regression model and catch anomalies as portions of the signal that the

model fails to reconstruct. Thus, we adopt the Isolation Forest model to detect anomalies from the reconstruction error time series. Finally, the scores of the detected anomalies are used to categorize the thermal activity level. The workflow of the proposed three-step approach is as follows (Figure 2):

1. Fit LST Time Series under "Normal" Conditions
   - Use the Non-linear Least Squares (NLS) Regression model to fit the LST time series under normal conditions.
   - Identify anomalies as portions of the signal that the model fails to reconstruct accurately.
2. Detect Anomalies Using the Isolation Forest Model
   - Adopt the Isolation Forest model to detect anomalies from the reconstruction error time series.
   - Utilize the Isolation Forest algorithm to efficiently identify outliers or anomalies in the data.
3. Categorize Thermal Activity Level Based on Anomaly Scores
   - Use the scores of the detected anomalies to categorize the thermal activity level.
   - Assign higher scores to anomalies indicating more significant deviations from the normal pattern, thereby prioritizing areas of heightened thermal activity.

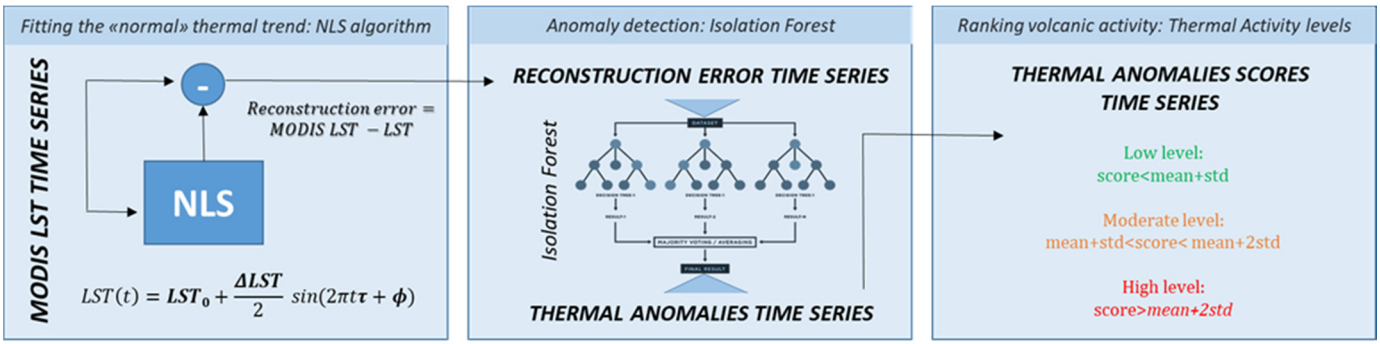

Figure 2. Workflow of the proposed three-step approach.

4.1. Fitting the "Normal" Thermal Trend: The NLS Algorithm

We expect that LST in normal conditions (without volcanic activity) exhibits seasonality influenced by a sinusoidal trend described by Stallman [54] as follows:

$$LST(t) = LST_0 + \frac{\Delta LST}{2}(2\pi t\tau + \phi) \quad (1)$$

where LST_0 represents the mean annual LST, ΔLST represents the amplitude between maximal and minimal LST, τ represents the period of oscillation of LST, and ϕ represents an offset needed to adjust the time (t) when LST(t) = LST_0. Thus, we estimate the values of LST_0, ΔLST, τ, and ϕ that best fit the MODIS LST time series collected in the previous step. This task is achieved by using the Levenberg–Marquardt algorithm [55], widely adopted as an optimization method to solve non-linear least squares problems.

Once we find LST_0, ΔLST, τ, and ϕ, we can estimate LST(t) that represents the average normal values at time t in ideal conditions. By computing the difference between MODIS LST and LST(t), we can estimate the reconstruction error, indicating how much the reality differs from the ideal condition. If the prediction error is small, it is highly probable that the current state is similar to the normal state, while a large prediction error suggests that the current state is abnormal. This difference accounts for random errors due to the weather variances, snow coverage, and external conditions affected by volcanic activity.

4.2. Anomaly Detection: Isolation Forest

The goal is to detect thermal anomalies associated with volcanic activity from the time series of the reconstructed error, filtering out random errors due to the weather variances and snow coverage. While random errors are low in magnitude with respect to volcanic activity, snow coverage may negatively affect negative reconstruction errors that are filtered out because they are not related to volcanic activities. The latter ones, in fact, are shown by the maximum positive values of reconstruction error. Thus, for each scene, we considered the maximum values of the reconstruction error, and we built the time series from the entire collection, which we inputted into an unsupervised machine learning algorithm to detect anomalies in the time series.

We employed the isolation forest machine learning algorithm since it is a popular unsupervised learning technique known for its effectiveness in detecting anomalies in large datasets. The isolation forest algorithm [56] detects anomalies by isolating anomalies from normal points using an ensemble of Isolation Trees. Each Isolation Tree is trained for a subset of training observations, sampled without replacements. The algorithm grows an Isolation Tree by choosing a split variable and split position at random until every observation in a subset lands in a separate leaf node. Anomalies are few and different; therefore, an anomaly lands in a separate leaf node closer to the root node and has a shorter path length (the distance from the root node to the leaf node) than normal points. The algorithm identifies anomalies using anomaly scores defined based on the average path lengths over all Isolation Trees. Anomalies are identified as instances that require fewer partitioning steps to isolate, reflecting their deviation from the norm. The Isolation Forest algorithm computes the anomaly score s(x) of an observation x by normalizing the path length h(x):

$$s(x) = 2^{-\frac{E(x)}{c(n)}} \quad (2)$$

where E[h(x)] is the average path length over all Isolation Trees in the Isolation Forest, and c(n) is the average path length of unsuccessful searches in a binary search tree of n observations. For each sample, the Isolation Forest returns a score bound between 0 and 1. The score approaches 1 as E[h(x)] approaches 0. Therefore, a score value close to 1 indicates an anomaly. The score approaches 0 as E[h(x)] approaches n–1. Also, the score approaches 0.5 when E[h(x)] approaches c(n). Therefore, a score value smaller than 0.5 and close to 0 indicates a normal sample.

4.3. Classifying Volcanic Activity: Thermal Activity Levels

For each thermal anomaly detected, a score is associated with the Isolation Forest's readiness to isolate the anomalies, indicating how anomalous the sample was compared to the closest observations. Based on the Isolation Forest score, we assign a thermal activity level to each sample. This assignment depends not only on the instantaneous thermal value but also on how much it differs from the other samples. To establish statistical thresholds, we utilized two volcanoes as study cases characterized by thermal activity spanning from low to high levels, namely Etna and Klyuchevskoy. We defined three thermal activity levels closely related to the level of concern arising from the volcanic activity. The low level is associated with baseline volcanic thermal activity leading to a low level of concern, including intracrater activity, unrest thermal signals, and fumarolic activity. The statistical threshold is score < mean + standard deviation (std). The moderate level associated with volcanic activity leads to a moderate level of concern, such as active lava domes, small overflow, and cooling lava flow. The statistical threshold is mean + std < score < mean + 2std. The high thermal activity level is associated with large overflows, active lava flows or paroxysm events, indicating a high level of concern. The statistical threshold is score > mean + 2std.

5. Results

For each of the volcanoes investigated, we present the results obtained by applying the proposed approach to the complete dataset covering the area of interest. Since the reconstruction error, as defined, represents the temperature above the temporal average (TAB), these two terms are used interchangeably. Figure 3 displays the results from the NLS fitting step to the anomaly detection step for one of the targeted volcanoes, namely Etna. Specifically, it includes the reconstructed signal over the real thermal signal (a), the reconstructed error (b), the detected anomalies (c), and the real thermal signal identified as anomalous (d). The temperature above average corresponds to the reconstructed error, defined as the difference between the real and reconstructed temperature of the detected anomalies. The time series of the temperature above average of the detected volcanic anomalies for all the volcanoes are shown in Figures 4 and 5. Blue arrows indicate the start of an eruption, while the gray shaded area indicates time windows characterized by an increase in activity preceding the eruption. Thermal activity levels for each volcano are displayed in Figure 6 in terms of low, moderate, and high levels.

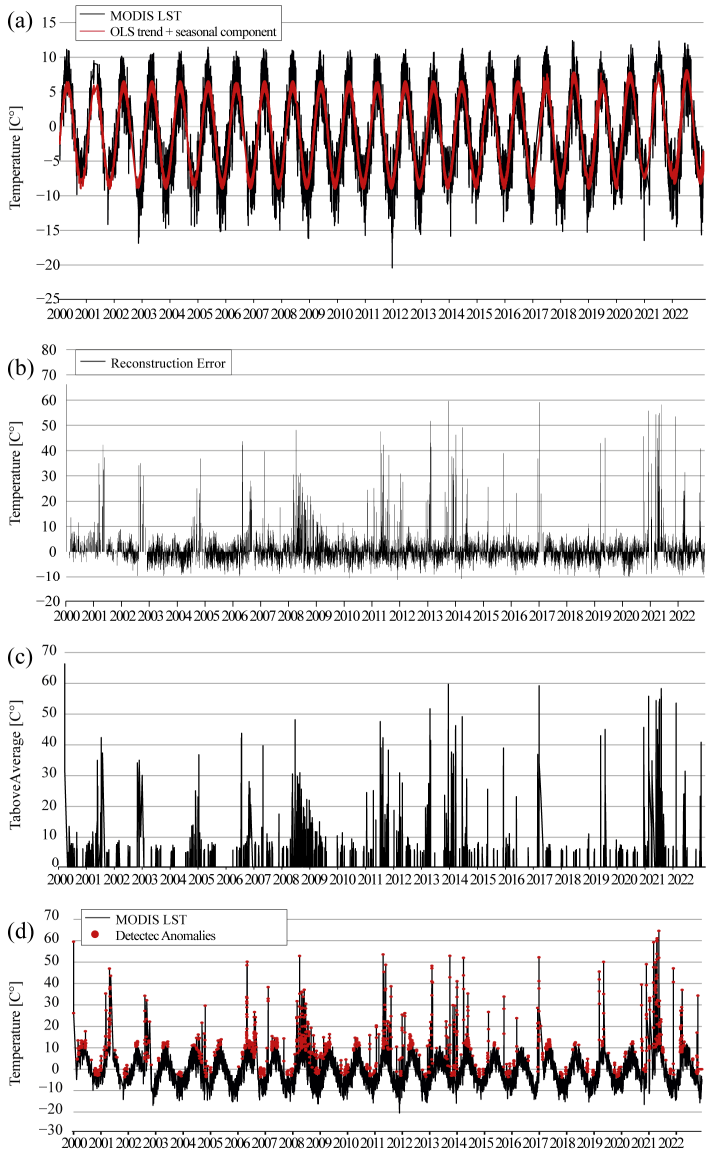

Figure 3. NLS adaptation phase to the anomaly detection phase for Etna. The reconstructed signal over the real thermal signal (**a**), the reconstructed error (**b**), the LST temperature of the detected anomalies (**c**), and the real thermal signal identified as anomalous over the real thermal signal (**d**).

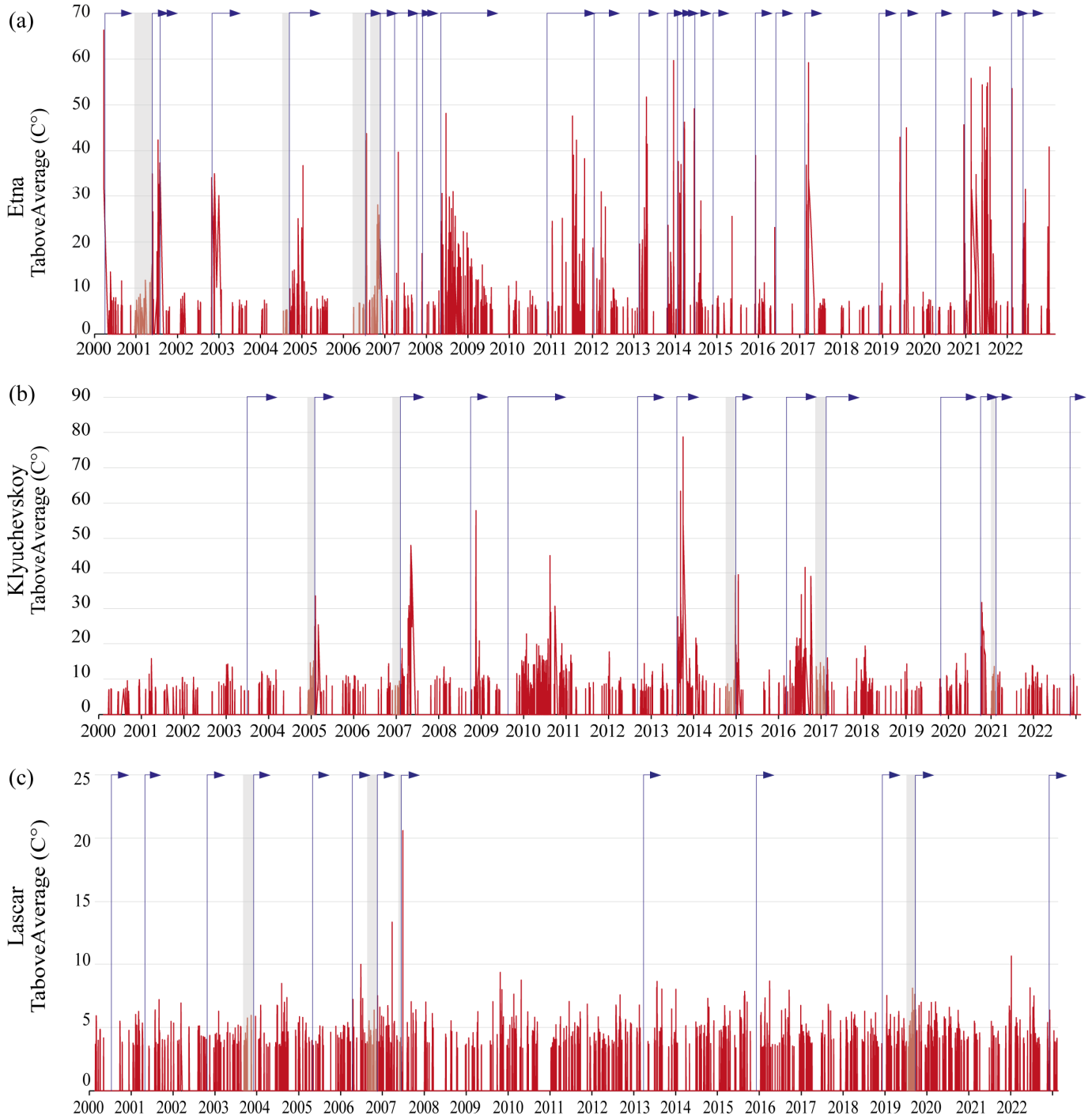

Figure 4. Time series of the temperature above average of the detected volcanic anomalies for Etna, Klyuchevskoy, and Lascar. Blue arrows indicate the starting of an eruption, while the gray shaded area indicates time windows characterized by an increase in activity preceding the eruption.

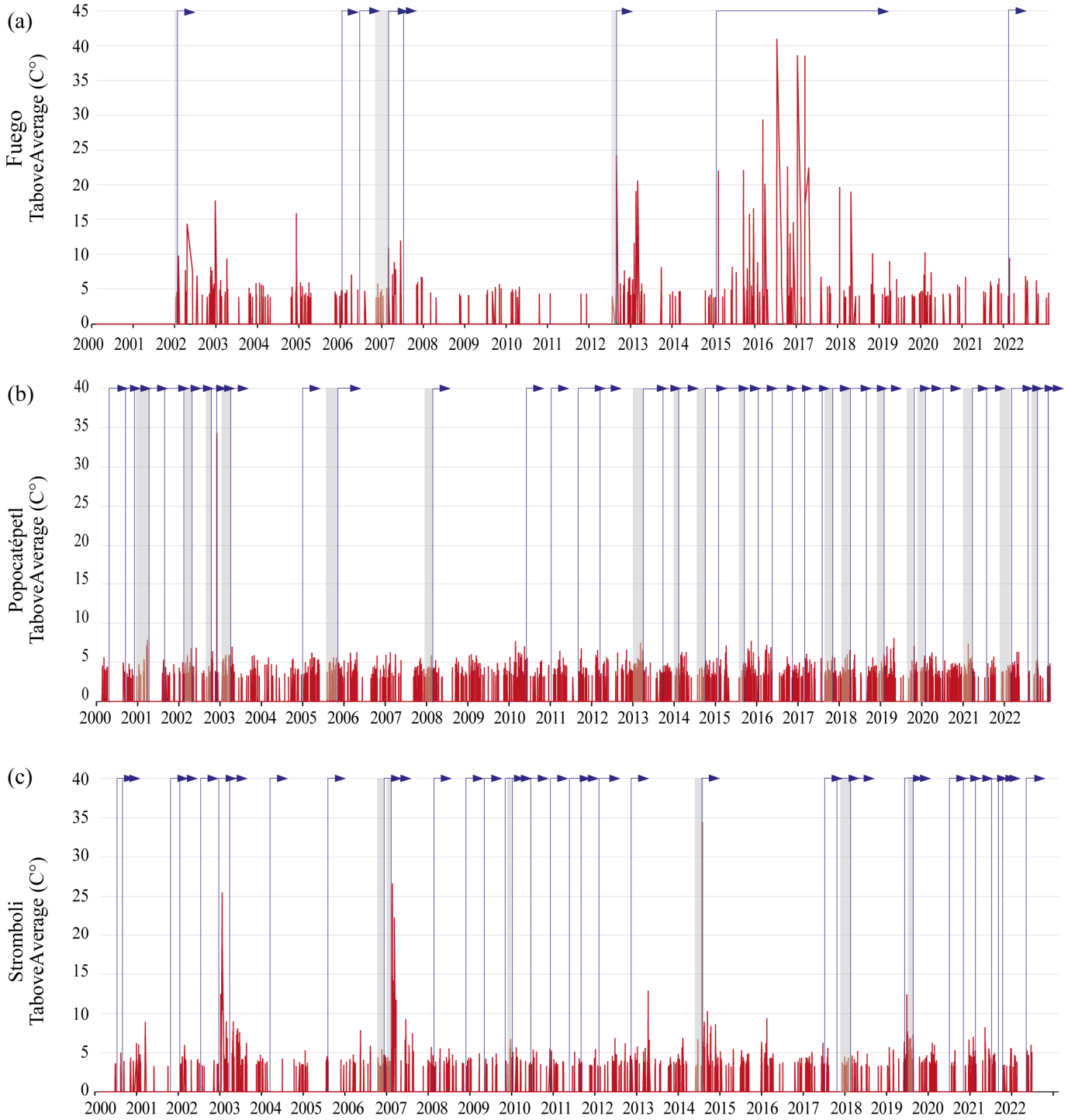

Figure 5. Time series of the temperature above average of the detected volcanic anomalies for Fuego, Popocatépetl, and Stromboli. Blue arrows indicate the starting of an eruption, while the gray shaded area indicates time windows characterized by an increase in activity preceding the eruption.

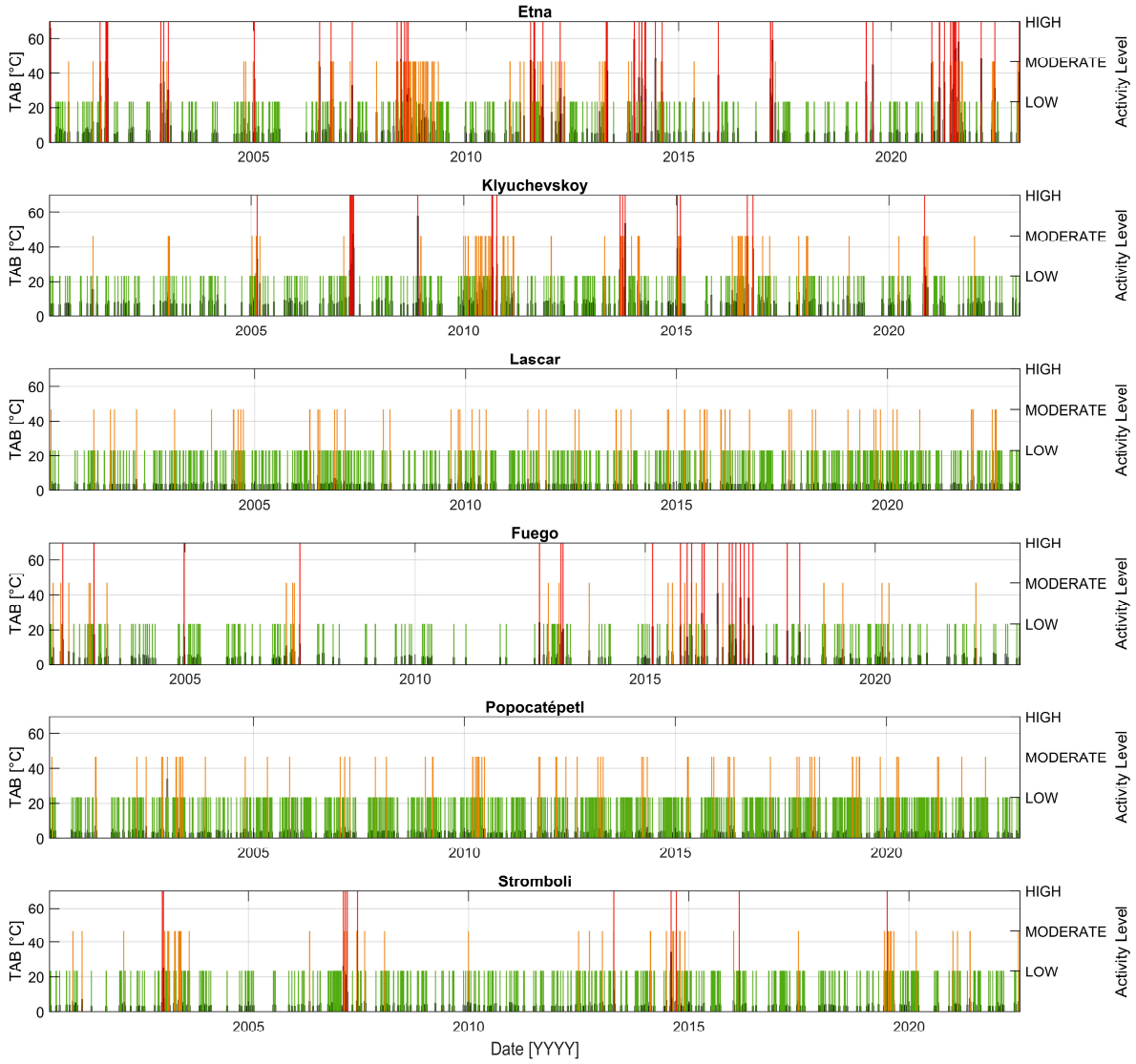

Figure 6. Time series of the temperature above average of the detected volcanic anomalies and the activity levels low (green bars), moderate (orange bars) and high (red bars) for Etna, Klyuchevskoy, Lascar, Fuego, Popocatépetl, and Stromboli.

6. Discussion

6.1. Thermal Anomaly Detection

The detection and monitoring of thermal anomalies play a crucial role in assessing volcanic hazards and mitigating potential risks associated with volcanic activity. Land surface temperature anomalies often indicate magma movement beneath the Earth's surface, which can lead to volcanic eruptions or other hazardous events [57]. For example, an increase in surface temperature, as indicated by thermal anomalies, may suggest magma ascent toward the volcano's summit, potentially leading to eruption. Furthermore, the persistence or intensification of thermal anomalies over time can signify sustained volcanic activity, increasing the likelihood of imminent eruption [58].

The results demonstrate that the thermal information provided by MODIS Land Surface Temperature (LST) combined with machine learning enables the detection of both pre-eruptive increases and, when satellite scenes are clear, the eruption itself (Figures 4 and 5). Etna is one of the most active volcanoes in the world located in a densely populated area, which underscores the paramount importance of detecting and monitoring thermal anoma-

lies. We explore multiple eruptive periods during which thermal anomalies were identified prior to eruptions (Figure 4a).

From 14 November 2000, an increase in thermal anomalies was observed at Etna until the end of July 2001. The initial anomaly corresponds to the activity of the Bocca Nuova crater [INGV internal report]. On 3 May 2001, a notable increase in thermal anomalies was evident (Figure 4a), aligning with heightened strombolian activity at the Sud Est crater preceding the paroxysm of 9 May 2001 (INGV internal report [43]). The anomaly persisted due to the ongoing effusive and explosive activity at the summit of Etna, reaching a peak on 3 June 2001 (Figure 4a), ahead of the paroxysmal event of 6 June 2001 [43]. Subsequently, eruptive activity continued with 16 lava fountains until 16 July. Lateral activity commenced on 17 July 2001 [43,59,60], which was detected and continuously monitored (Figure 4a). On 7 September 2004, significant lateral activity began, lasting until 8 March 2005 [43,61], accompanied by an increase in thermal anomaly observed from late July 2004 (Figure 4a). This thermal anomaly persisted throughout the development of the lava field until it completely cooled. A new lateral activity commenced on 15 July 2006, lasting until 27 July 2006. A notable increase in thermal anomaly was observed from late March 2006 preceding effusive activity (Figure 4a). Shortly after the conclusion of lateral effusive activity, another thermal anomaly was detected from late August 2006 (Figure 4a). The thermal anomaly intensified until peaking at the paroxysm of 16 November 2006, followed by a series of lava fountains (nine in total) [43], until May 2007 (INGV internal report [43]). Thermal anomalies were also identified throughout the period of paroxysmal events.

Klyuchevskoy volcano stands as one of the world's most active volcanoes. Given the extreme weather conditions in the region, monitoring infrastructure primarily relies on seismic stations and webcams. Therefore, the study of thermal anomalies from satellites holds fundamental importance in understanding the eruptive activity of Klyuchevskoy volcano. We discuss the increase in thermal anomalies during two eruptive periods (Figure 4b). On 14 January 2005, following a year of quiescence, strombolian activity commenced from the summit of Klyuchevskoy [44,62]. The activity evolved into effusive activity by the end of January. The onset of this effusive activity was preceded by an increase in seismicity and sightings of brilliance within the crater [63]. Satellite images from 5 January 2005 captured an escalation in the thermal anomalies, peaking at the initiation of strombolian activity and persisting until the conclusion of summit activity (Figure 4b). Following almost two years of quiescence, the summit strombolian eruption on 18 March 2007 was preceded by an increase in thermal anomaly recorded from 29 January 2007 until the termination of the eruption (Figure 4b). Two days prior, luminescence and bomb ejections were observed above the central crater [63]. The eruption proceeded with volcanic activity and lava flow emission until 18 June 2007.

Lascar is considered the most active volcano in the Central Andean Volcanic Zone, characterized by continuous degassing. We discuss two cases: one where the crescendo of the thermal anomaly predicts an eruptive event and another where there is a thermal anomaly without an eruptive event (Figure 4c). On 11 September 2019, a northwest dispersing gas plume was identified on a satellite image, accompanied by a pronounced peak in the thermal radiance [64]. An increase in the thermal anomaly was detected in the days immediately preceding the eruption (Figure 4c), although there is no information in the literature about signs preceding the eruption (e.g., an increase in seismic tremor). In early January 2022, the satellite data showed a peak thermal anomaly not associated with an eruption (Figure 4c). SERNAGEOMIN reports visible luminescence from the crater starting on 11 January, which continued for the next few days ([63]; Servicio Nacional de Geología y Minería https://www.sernageomin.cl/; accessed on 4 March 2024). At the same time, a more frequent emission of gas and steam was detected than in previous months [63].

Fuego is currently the most active volcanic center of the Fuego–Acatenango massif. Its eruptive activity has been characterized by strombolian and effusive events, as well as some paroxysmal events, which have caused considerable inconvenience to surrounding communities [65]. We discuss two paroxysmal events that were preceded by an increase

in thermal anomalies (Figure 5a). Since the end of January 2002, an increase in thermal anomaly has been detected. On 1 February, strombolian activity was observed, accompanied by the production of ash, steam, and lava flow [63]. The peak of the anomaly coincides with the paroxysmal event of 9 February 2002. The paroxysm of 13 September 2012 is preceded and followed by a long period of no paroxysm [63,66]. This event was preceded 48 h earlier by an increase in seismic tremor and the emission of a lava flow. Additionally, a thermal anomaly was detected from 7 August, which peaked on the day of the paroxysmal event (Figure 5a).

The ongoing eruptive activity of Popocatépetl volcano has been characterized by emplacement and subsequent destruction of a succession of lava domes. We analyze two cases in which the increase in thermal anomalies precedes the destruction of the lava domes. On 28 February 2001, a new lava dome began to be emplaced at the bottom of the crater floor [48]. Its growth was accompanied by an increase in seismic tremor and small to moderate steam emissions [63]. A thermal anomaly was detected from early March, increasing until the destruction of the lava dome (Figure 5b). Another thermal anomaly was detected from early 2013 (Figure 5b). On 10 February 2023, a lava dome began to form inside the crater, accompanied by an increase in seismic tremor [48,63]. The thermal anomaly continued to grow until it reached its peak coinciding with the destruction of the lava dome on 15 April 2015 [48] (Figure 5b). Additionally, eruptive activity was preceded by an increase in seismic tremor and ash emissions [48,63].

The persistent normal activity of Stromboli is occasionally interrupted by sudden and highly energetic explosive events called strombolian paroxysms. We analyze one case in which the increase in thermal anomalies precedes effusive activity and another case in which the increase in thermal anomalies does not precede any activity (Figure 5c). A new effusive activity period at Stromboli started on 6 August 2014. This event was preceded by two months of high-intensity eruptive activity, characterized by frequent and strong explosions and overflows [67,68]. From the beginning of June, the first temperature anomalies were detected, peaking on 7 August 2014 (Figure 5c). In April 2013, there was a peak thermal anomaly (Figure 5c), although no paroxysmal or major activity is reported in the literature. A significant increase in CO_2 flux from the craters is reported by Inguaggiato et al. [69].

6.2. Thermal Activity Levels

Results show that the combined use of LST measurements and unsupervised Isolation Forest algorithm aids not only in monitoring volcanic eruptions but also in detecting subtle thermal changes that may precede them, as shown in Figures 4 and 5. Four eruptions at Etna showed a pre-eruptive change in trend (Figure 4a), the Klyuchevskoy eruption exhibited six types of identifiable pre-eruptive changes in trend (Figure 4b), and three periods of increased pre-eruption thermal anomaly were also identified in the case of Lascar (Figure 4c). In addition, three pre-eruptive changes at Fuego were identified (Figure 5a), and at Stromboli, four cases were identified in which the growth of the thermal anomaly preceded an eruptive event (Figure 5c). Instead, at Popocatépetl, 18 changes in trend were detected (Figure 5b). It was noted that in volcanoes subject to continuous outgassing or persistent activity (e.g., Etna, Lascar, Fuego, Stromboli), the detection of pre-eruptive thermal anomalies is limited. Thus, the analysis of thermal anomalies from satellite data emerges as a crucial and reliable tool for predicting volcanic eruptions. A significant increase in thermal anomalies was detected before the onset of eruptive activity, providing a valuable window for early warning and forecasting volcanic hazards.

Thermal anomalies are valuable indicators of volcanic eruptive phenomena, such as lava effusions, volcanic gas emissions, and the formation of volcanic domes or lava lakes [70]. Ramsey et al. [42] successfully retrieved mean temperature, maximum temperature, and heat flux from high-spatial-resolution satellite data using unsupervised machine learning techniques. While medium spatial resolution data may lack the same spatial accuracy, collecting more images over time enables gathering more information

on a specific volcano. Each thermal anomaly sample incorporates both the intensity and area information. Isolation Forest outcomes help filter significant changes in LST from historical time series data, facilitating further investigation into the eruptive history and associating each detected anomaly with a volcanic activity phase. By establishing statistical thresholds from active volcanic study cases such as Etna and Klyuchevskoy, activity levels (low, moderate, high) were estimated and applied to classify volcanic activity levels across all studied volcanoes. Figure 6 illustrates the results of this analysis, demonstrating that utilizing unsupervised Isolation Forest machine learning allows for not only detecting main phases of volcanic eruptive history, but also automatically discriminating their volcanic phases. Notably, the activity levels found for the investigated volcanoes align with previous research [42]. Generally, Etna, Klyuchevskoy, Stromboli, and Fuego exhibit all three activity levels, ranging from degassing (low level) to lava flows and paroxysmal activity (high level), whereas Lascar and Popocatépet show mainly low and moderate levels due to continuous degassing or dome formation [47,48].

For example, on Etna, a series of paroxysmal events began on 16 November 2006, with pre-eruptive changes detected and classified by the Isolation Forest machine learning technique, identifying phases of moderate activity (strombolian activity) and high thermal activity associated with a lava flow preceding the lava fountaining activity [INGV internal report]. Similar pre-eruptive changes were observed during the January 2005 and March 2007 eruptions of Klyuchevskoy volcano (Figure 6), where the Isolation Forest algorithm identified pre-eruptive changes and paroxysmal phases. While the 2007 pre-eruptive changes were already identified in the work of Coppola et al. [62], it is noteworthy that using Isolation Forest and LST data, changes were observed before the 16 January 2005 eruption, as early as 21 December 2004. Specifically, moderate-level activity was identified on 8 January 2005. On the other hand, in the case of Lascar, the Isolation Forest recorded two periods of moderate activity in July 2006 and April 2007. However, there is no information on these periods of volcanic activity, likely due to the poor monitoring of the volcano. It is therefore presumed that these periods were characterized by strombolian activity or dome explosions, typical of Lascar volcano [47]. In the case of the eruption on 1 December 2005 at Popocatépetl (Figure 6), the Isolation Forest also successfully detected the main pre-eruptive phases of dome-building activity before its destruction. Lastly, by observing and comparing the charts of thermal anomalies (Figure 5c) and the Isolation Forest results (Figure 6) at Stromboli, the Isolation Forest algorithm also identified the strombolian activity preceding the paroxysm of 28 August 2019.

7. Conclusions

Satellite Land Surface Temperature (LST) measurements offer a valuable means of continuously monitoring volcanic regions, providing insights into a range of volcanic phenomena from subtle thermal changes due to gas emissions to active lava flows.

By leveraging the capabilities of GEE and the isolation forest algorithm, we were able to efficiently detect and analyze thermal anomalies associated with volcanic activity. The approach proposed in this study demonstrated its effectiveness in capturing significant trends from historical time series data. By employing an unsupervised machine learning (ML) algorithm on these time series, significant temperature changes, including pre-eruptive indicators and actual volcanic eruptions, can be automatically identified without external bias. Utilizing Isolation Forest score parameters, we were able to classify the thermal activity level, thereby associating the thermal state of the volcano with the level of concern regarding ongoing volcanic activity.

The inclusion of six volcanoes with diverse characteristics in our analysis demonstrates the versatility and applicability of our proposed approach on a global scale. This underscores the potential for widespread adoption and implementation of this methodology in volcanic monitoring efforts worldwide. Furthermore, the scalability of our approach allows for seamless integration into existing monitoring frameworks, enhancing their capabilities and effectiveness in identifying and assessing volcanic hazards.

The timely detection and characterization of thermal anomalies through satellite observations play a crucial role in assessing volcanic hazards. Detecting pre-eruptive thermal anomalies from satellites can be used for real-time monitoring, especially in areas with little or no ground-based monitoring systems. This approach is a valuable tool to integrate into existing warning systems operated by volcanic observatories to forecast volcanic hazards. Despite limitations such as cloud cover and poor temporal resolution (e.g., satellite passages may not coincide with short eruption events), the Isolation Forest machine learning algorithm can maximize the utility of thermal infrared satellite data to provide time-critical hazard information. This algorithm helps to identify and classify anomaly thermal activity, improving the reliability and accuracy of volcanic monitoring.

Classifying the thermal activity level is critical for understanding the thermal state of the volcano, enabling real-time hazard assessment. By providing early warning and detailed insights into volcanic activity, these observations enable authorities to implement appropriate measures for forecasting and monitoring volcanic hazards in affected areas. This proactive approach enhances overall preparedness and resilience in regions susceptible to volcanic activity, ultimately contributing to the safety and well-being of surrounding communities. Moreover, continuous monitoring facilitated by satellite observations ensures that authorities can dynamically adapt their response strategies, thereby minimizing the potential impact of volcanic events on human lives and infrastructure.

Author Contributions: Conceptualization, C.C. and A.B.M.; methodology, C.C.; software, C.C. and A.B.M.; validation, M.S.R.; formal analysis, C.C. and A.B.M.; data curation, C.C. and A.B.M.; writing—original draft preparation, C.C. and A.B.M.; writing—review and editing, C.D.N. and M.S.R.; visualization, A.B.M.; supervision, C.D.N.; project administration, C.D.N.; funding acquisition, C.D.N. All authors have read and agreed to the published version of the manuscript.

Funding: This research was funded by the ATHOS Research Programme (INGV OB.FU. 0867.010), by the 2019 Strategic Project FIRST—Forecasting Eruptive activity at Stromboli volcano: timing, eruptive style, size, intensity, and duration—of the INGV Volcanoes Department (Delibera n. 144/2020), and by Project INGV Pianeta Dinamico VT_ORME 2023–2025 (INGV OB.FU. 1020.010). The work was also partially supported by the Fulbright Visiting Research Program awarded to C.C., which allowed her to spend six months in the Department of Geology and Environmental Science of Pittsburgh, University of Pittsburgh.

Data Availability Statement: All MODIS data utilized in this work are available on Google Earth Engine.

Acknowledgments: This work was developed within the framework of the Laboratory of Technologies for Volcanology (TechnoLab) at the INGV in Catania (Italy). We are grateful to NASA for MODIS data. Note: Google CoLaboratory™ is a trademark of Google LLC—©2018 Google LLC All rights reserved.

Conflicts of Interest: The authors declare no conflicts of interest. The funders had no role in the design of the study; in the collection, analyses, or interpretation of data; in the writing of the manuscript; or in the decision to publish the results.

References

1. Harris, A.; Chevrel, O.; Coppola, D.; Ramsey, M.; Hrysiewicz, A.; Thivet, S.; Villeneuve, N.; Favalli, M.; Peltier, A.; Kowalski, P.; et al. Validation of an integrated satellite-data-driven response to an effusive crisis: The April–May 2018 eruption of Piton de la Fournaise. *Ann. Geophys.* **2019**, *61*, AC48. [CrossRef]
2. Calvari, S.; Spampinato, L.; Lodato, L.; Harris AJ, L.; Patrick, M.R.; Dehn, J.; Burton, M.R.; Andronico, D. Chronology and complex volcanic processes during the 2002–2003 flank eruption at Stromboli volcano (Italy) reconstructed from direct observations and surveys with a handheld thermal camera. *J. Geophys. Res.* **2005**, *110*, B02201. [CrossRef]
3. Watson, I.M.; Realmuto, V.J.; Rose, W.; Prata, A.; Bluth, G.; Gu, Y.; Yu, T. Thermal infrared remote sensing of volcanic emissions using the moderate resolution imaging spectro-radiometer (MODIS). *J. Volcanol. Geotherm. Res.* **2004**, *135*, 75–89. [CrossRef]
4. Moussallam, Y.; Bani, P.; Schipper, C.I.; Cardona, C.; Franco, L.; Barnie, T.; Amigo, A.; Curtis, A.; Peters, N.; Aiuppa, A.; et al. Unrest at the Nevados de Chillán volcanic complex: A failed or yet to unfold magmatic eruption? *Volcanica* **2018**, *1*, 19–32. [CrossRef]

5. Corradino, C.; Ganci, G.; Cappello, A.; Bilotta, G.; Hérault, A.; Del Negro, C. Mapping Recent Lava Flows at Mount Etna Using Multispectral Sentinel-2 Images and Machine Learning Techniques. *Remote Sens.* **2019**, *11*, 1916. [CrossRef]
6. Corradino, C.; Amato, E.; Torrisi, F.; Calvari, S.; Del Negro, C. Classifying Major Explosions and Paroxysms at Stromboli Volcano (Italy) from Space. *Remote Sens.* **2021**, *13*, 4080. [CrossRef]
7. Corradino, C.; Bilotta, G.; Cappello, A.; Fortuna, L.; Del Negro, C. Combining Radar and Optical Satellite Imagery with Machine Learning to Map Lava Flows at Mount Etna and Fogo Island. *Energies* **2021**, *14*, 197. [CrossRef]
8. Corradino, C.; Amato, E.; Torrisi, F.; Del Negro, C. Towards an automatic generalized machine learning approach to map lava flows. In Proceedings of the 17th International Workshop on Cellular Nanoscale Networks and their Applications (CNNA), Catania, Italy, 29 September–1 October 2021; pp. 1–4. [CrossRef]
9. Corradino, C.; Amato, E.; Torrisi, F.; Del Negro, C. Data-Driven Random Forest Models for Detecting Volcanic Hot Spots in Sentinel-2 MSI Images. *Remote Sens.* **2022**, *14*, 4370. [CrossRef]
10. Ganci, G.; Cappello, A.; Bilotta, G.; Del Negro, C. How the Variety of Satellite Remote Sensing Data over Volcanoes Can Assist Hazard Monitoring Efforts: The 2011 Eruption of Nabro Volcano. *Remote Sens. Environ.* **2020**, *236*, 111426. [CrossRef]
11. Amato, E.; Corradino, C.; Torrisi, F.; Del Negro, C. Mapping lava flows at Etna Volcano using Google Earth Engine, open-access satellite data, and machine learning. In Proceedings of the 2021 International Conference on Electrical, Computer, Communications and Mechatronics Engineering (ICECCME), Mauritius, Mauritius, 7–8 October 2021; pp. 1–6. [CrossRef]
12. Amato, E.; Corradino, C.; Torrisi, F.; Del Negro, C. Combined Use of Satellite Data and Machine Learning for Detecting, Measuring, and Monitoring Active Lava Flows at Etna Volcano. *Authorea* **2021**. [CrossRef]
13. Amato, E.; Corradino, C.; Torrisi, F.; Del Negro, C. A Deep Convolutional Neural Network for Detecting Volcanic Thermal Anomalies from Satellite Images. *Remote Sens.* **2023**, *15*, 3718. [CrossRef]
14. Amato, E.; Corradino, C.; Torrisi, F.; Del Negro, C. Spectral analysis of lava flows: Temporal and physicochemical effects. *Il Nuovo C. C SIF Congr.* **2022**, *46*, 144. [CrossRef]
15. Amato, E.; Zago, V.; Del Negro, C. A physically consistent AI-based SPH emulator for computational fluid dynamics. *Nonlinear Eng. Model. Appl.* **2024**, *13*, 20220359. [CrossRef]
16. Torrisi, F. Automatic detection of volcanic ash clouds using MSG-SEVIRI satellite data and machine learning techniques. *Il Nuovo C. C* **2022**, *45*, 4.
17. Torrisi, F.; Amato, E.; Corradino, C.; Mangiagli, S.; Del Negro, C. Characterization of Volcanic Cloud Components Using Machine Learning Techniques and SEVIRI Infrared Images. *Sensors* **2022**, *22*, 20. [CrossRef]
18. Torrisi, F.; Amato, E.; Corradino, C.; Del Negro, C. The FastVRP automatic platform for the thermal monitoring of volcanic activity using VIIRS and SLSTR sensors: FastFRP to monitor volcanic radiative power. *Ann. Geophys.* **2023**, *65*, 1. [CrossRef]
19. Torrisi, F.; Corradino, C.; Cariello, S.; Del Negro, C. Enhancing detection of volcanic ash clouds from space with convolutional neural networks. *J. Volcanol. Geotherm. Res.* **2024**, *448*, 108046. [CrossRef]
20. Del Negro, C.; Amato, E.; Torrisi, F.; Corradino, C.; Bucolo, M.; Fortuna, L. Support Vector Machine for volcano hazard monitoring from space at Mount Etna. In Proceedings of the 2022 IEEE Mediterranean Electrotechnical Conference (MELECON), Palermo, Italy, 14–16 June 2022; pp. 627–631. [CrossRef]
21. Cariello, S.; Corradino, C.; Torrisi, F.; Del Negro, C. Cascading Machine Learning to Monitor Volcanic Thermal Activity Using Orbital Infrared Data: From Detection to Quantitative Evaluation. *Remote Sens.* **2024**, *16*, 171. [CrossRef]
22. Wright, R.; Flynn, L.P.; Garbeil, H.; Harris, A.J.; Pilger, E. MODVOLC: Near-real-time thermal monitoring of global volcanism. *J. Volcanol. Geotherm. Res.* **2004**, *135*, 29–49. [CrossRef]
23. Gouhier, M.; Guéhenneux, Y.; Labazuy, P.; Cacault, P.; Decriem, J.; Rivet, S. HOTVOLC: A web-based monitoring system for volcanic hot spots. *Geol. Soc. Lond. Spec. Publ.* **2016**, *426*, 223–241. [CrossRef]
24. Davies, D.; Ederer, G.; Olsina, O.; Wong, M.; Cechini, M.; Boller, R. NASA's Fire Information for Resource Management System (FIRMS): Near Real-Time Global Fire Monitoring Using Data from MODIS and VIIRS. NASA Technical Reports. 3 October 2019. Available online: https://ntrs.nasa.gov/search.jsp?R=20190032007 (accessed on 2 March 2024).
25. Coppola, D.; Laiolo, M.; Cigolini, C.; Massimetti, F.; Delle Donne, D.; Ripepe, M.; Arias, H.; Barsotti, S.; Parra, C.B.; Centeno, R.G.; et al. Thermal remote sensing for global volcano monitoring: Experiences from the MIROVA system. *Front. Earth Sci.* **2020**, *7*, 362. [CrossRef]
26. Vicari, A.; Bilotta, G.; Bonfiglio, S.; Cappello, A.; Ganci, G.; Hérault, A.; Rustico, E.; Gallo, G.; Del Negro, C. LAV@ HAZARD: A web-GIS interface for volcanic hazard assessment. *Ann. Geophys.* **2011**, *53*, 1.
27. Corradino, C.; Ramsey, M.S.; Pailot-Bonnetat, S.; Harris, A.J.L.; Del Negro, C. Detection of Subtle Thermal Anomalies: Deep Learning Applied to the ASTER Global Volcano Dataset. *IEEE Trans. Geosci. Remote Sens.* **2023**, *61*, 1–15. [CrossRef]
28. Moussallam, Y.; Oppenheimer, C.; Scaillet, B. On the relationship between oxidation state and temperature of volcanic gas emissions. *Earth Planet. Sci. Lett.* **2019**, *520*, 260–267. [CrossRef]
29. Wright, R.; Flynn, L.; Garbeil, H.; Harris, A.; Pilger, E. Automated volcanic eruption detection using MODIS. *Remote Sens. Environ.* **2002**, *82*, 135–155. [CrossRef]
30. Girona, T.; Realmuto, V.; Lundgren, P. Large-scale thermal unrest of volcanoes for years prior to eruption. *Nat. Geosci.* **2021**, *14*, 238–241. [CrossRef]

31. Wan, D.; Xiao, Y.; Zhang, P.; Feng, J.; Zhu, Y.; Liu, Q. Hydrological Time Series Anomaly Mining Based on Symbolization and Distance Measure. In Proceedings of the 2014 IEEE International Congress on Big Data, Anchorage, AK, USA, 27 June 2014–2 July 2014; pp. 339–346. [CrossRef]
32. Aliano, C.; Corrado, R.; Filizzola, C.; Genzano, N.; Pergola, N.; Tramutoli, V. Robust TIR satellite techniques for monitoring earthquake active regions: Limits, main achievements and perspectives. *Ann. Geophys.* **2008**, *51*, 303–317. [CrossRef]
33. Lisi, M.; Filizzola, C.; Genzano, N.; Paciello, R.; Pergola, N.; Tramutoli, V. Reducing atmospheric noise in RST analysis of TIR satellite radiances for earthquakes prone areas satellite monitoring. *Phys. Chem. Earth Parts A/B/C* **2015**, *85*, 87–97. [CrossRef]
34. Mahmood, I.; Iqbal, M.F.; Shahzad, M.I.; Qaiser, S. Investigation of atmospheric anomalies associated with Kashmir and Awaran Earthquakes. *J. Atmos. Sol.-Terr. Phys.* **2017**, *154*, 75–85. [CrossRef]
35. Qin, K.; Wu, L.X.; Ouyang, X.Y.; Shen, X.H.; Zheng, S. Surface latent heat flux anomalies quasi-synchronous with ionospheric disturbances before the 2007 Pu'er earthquake in China. *Adv. Space Res.* **2014**, *53*, 266–271. [CrossRef]
36. Wu, L.; Zheng, S.; De Santis, A.; Qin, K.; Di Mauro, R.; Liu, S.; Rainone, M.L. Geosphere coupling and hydrothermal anomalies before the 2009 Mw 6.3 L'Aquila earthquake in Italy. *Nat. Hazards Earth Syst. Sci.* **2016**, *16*, 1859–1880. [CrossRef]
37. Genzano, N.; Filizzola, C.; Paciello, R.; Pergola, N.; Tramutoli, V. Robust Satellite Techniques (RST) for monitoring earthquake prone areas by satellite TIR observations: The case of 1999 Chi-Chi earthquake (Taiwan). *J. Asian Earth Sci.* **2015**, *114*, 289–298. [CrossRef]
38. Lisi, M.; Filizzola, C.; Genzano, N.; Grimaldi, C.S.L.; Lacava, T.; Marchese, F.; Mazzeo, G.; Pergola, N.; Tramutoli, V. A study on the Abruzzo 6 April 2009 earthquake by applying the RST approach to 15 years of AVHRR TIR observations. *Nat. Hazards Earth Syst. Sci.* **2010**, *10*, 395–406. [CrossRef]
39. Pergola, N.; Aliano, C.; Coviello, I.; Filizzola, C.; Genzano, N.; Lacava, T.; Lisi, M.; Mazzeo, G.; Tramutoli, V. Using RST approach and EOS-MODIS radiances for monitoring seismically active regions: A study on the 6 April 2009 Abruzzo earthquake. *Nat. Hazards Earth Syst. Sci.* **2010**, *10*, 239–249. [CrossRef]
40. Tramutoli, V.; Cuomo, V.; Filizzola, C.; Pergola, N.; Pietrapertosa, C. Assessing the potential of thermal infrared satellite surveys for monitoring seismically active areas: The case of Kocaeli (Izmit) earthquake, August 17, 1999. *Remote Sens. Environ.* **2005**, *96*, 409–426. [CrossRef]
41. Hill, D.J.; Minsker, B.S. Anomaly detection in streaming environmental sensor data: A data-driven modeling approach. *Environ. Model. Softw.* **2010**, *25*, 1014–1022. [CrossRef]
42. Ramsey, M.S.; Corradino, C.; Thompson, J.O.; Leggett, T.N. Statistical retrieval of volcanic activity in long time series orbital data: Implications for forecasting future activity. *Remote Sens. Environ.* **2023**, *295*, 113704. [CrossRef]
43. Andronico, D.; Cannata, A.; Di Grazia, G.; Ferrari, F. The 1986–2021 paroxysmal episodes at the summit craters of Mt. Etna: Insights into volcano dynamics and hazard. *Earth-Sci. Rev.* **2021**, *220*, 103686. [CrossRef]
44. Ozerov, A.Y. The evolution of high-alumina basalts of the Klyuchevskoy volcano, Kamchatka, Russia, based on microprobe analyses of mineral inclusions. *J. Volcanol. Geotherm. Res.* **2000**, *95*, 65–79. [CrossRef]
45. Tassi, F.; Aguilera, F.; Vaselli, O.; Medina, E.; Tedesco, D.; Delgado Huertas, A.; Poreda, R.; Kojima, S. The magmatic- and hydrothermal-dominated fumarolic system at the Active Crater of Lascar volcano, northern Chile. *Bull. Volcanol.* **2009**, *71*, 171–183. [CrossRef]
46. Gardeweg, M.; Amigo, A.; Matthews, R.; Clavero, J. Geología del Volcán Lascar, Región de Antofagasta. *Sernageomin* **2011**, *131*, 40.
47. Matthews, S.; Gardeweg, M.; Sparks, R. The 1984 to 1996 cyclic activity of Lascar Volcano, northern Chile: Cycles of dome growth, dome subsidence, degassing and explosive eruptions. *Bull. Volcanol.* **1997**, *59*, 72–82. [CrossRef]
48. Gómez-Vazquez, A.; De la Cruz-Reyna, S.; Mendoza-Rosas, A.T. The ongoing dome emplacement and destruction cyclic process at Popocatépetl volcano, Central Mexico. *Bull. Volcanol.* **2016**, *78*, 58. [CrossRef]
49. Lyons, J.J.; Waite, G.P.; Rose, W.I.; Chigna, G. Patterns in open vent, strombolian behavior at Fuego volcano, Guatemala, 2005-2007. *Bull. Volcanol.* **2010**, *72*, 1–15. [CrossRef]
50. Escobar Wolf, R.P. Volcanic Processes and Human Exposure as Elements to Build a Risk Model for Volcan de Fuego, Guatemala. Ph.D. Thesis, Michigan Technological University, Houghton, MI, USA, 2013.
51. Rosi, M.; Bertagnini, A.; Landi, P. Onset of the persistent activity at Stromboli Volcano (Italy). *Bull. Volcanol.* **2000**, *62*, 294–300. [CrossRef]
52. Barberi, F. Volcanic hazard assessment at Stromboli based on review of historical data. *Acta Vulcanol.* **1993**, *3*, 173–187.
53. Gorelick, N.; Hancher, M.; Dixon, M.; Ilyushchenko, S.; Thau, D.; Moore, R. Google Earth Engine: Planetary-scale geospatial analysis for everyone. *Remote Sens. Environ.* **2017**, *202*, 18–27. [CrossRef]
54. Stallman, R.W. Steady one-dimensional fluid flow in a semi-infinite porous medium with sinusoidal surface temperature. *J. Geophys. Res.* **1965**, *70*, 2821–2827. [CrossRef]
55. More, J.J. The Levenberg-Marquardt Algorithm: Implementation and Theory. In *Numerical Analysis: Proceedings of the Biennial Conference Held at Dundee, June 28–July 1, 1977*; Springer Berlin Heidelberg: Berlin/Heidelberg, Germany, 2006; pp. 105–116.
56. Liu, F.T.; Ting, K.M.; Zhou, Z. Isolation Forest. In Proceedings of the 2008 Eighth IEEE International Conference on Data Mining, Pisa, Italy, 15–19 December 2008; pp. 413–422.
57. Feldman, A.F.; Short Gianotti, D.J.; Trigo, I.F.; Salvucci, G.D.; Entekhabi, D. Satellite-based assessment of land surface energy partitioning-soil moisture relationships and effects of confounding variables. *Water Resour. Res.* **2019**, *55*, 10657–10677. [CrossRef]

58. Carn, S.A.; Clarisse, L.; Prata, A.J. Multi-decadal satellite measurements of global volcanic degassing. *J. Volcanol. Geotherm. Res.* **2016**, *311*, 99–134. [CrossRef]
59. Coltelli, M.; Proietti, C.; Branca, S.; Marsella, M.; Andronico, D.; Lodato, L. Analysis of the 2001 lava flow eruption of Mt. Etna from three-dimensional mapping. *J. Geophys. Res. Earth Surf.* **2007**, *112*, F02029. [CrossRef]
60. De Beni, E.; Cantarero, M.; Neri, M.; Messina, A. Lava flows of Mt Etna, Italy: The 2019 eruption within the context of the last two decades (1999–2019). *J. Maps* **2021**, *17*, 65–76. [CrossRef]
61. Fornaciai, A.; Andronico, D.; Favalli, M.; Spampinato, L.; Branca, S.; Lodato, L.; Bonforte, A.; Nannipieri, L. The 2004-05 Mt. Etna compound lava flow field: A retrospective analysis by combining remote and field methods. *J. Geophys. Res.-Solid Earth* **2021**, *126*, e2020JB020499. [CrossRef]
62. Coppola, D.; Laiolo, M.; Massimetti, F.; Hainzl, S.; Shevchenko, A.V.; Mania, R.; Shapiro, N.M.; Walter, T.R. Thermal remote sensing reveals communication between volcanoes of the Klyuchevskoy Volcanic Group. *Sci. Rep.* **2021**, *11*, 13090. [CrossRef]
63. Global Volcanism Program. Volcanoes of the World (v. 5.1.6). Available online: https://volcano.si.edu/ (accessed on 4 March 2024).
64. Ai, L.; Walter, T.R.; Aguilera, F.; Layana, S.; Mania, R.; Kujawa, C.; Zimmer, M.; Inostroza, M. Crater morphology, nested ring structures, and temperature anomalies studied by unoccupied aircraft system data at Lascar volcano, northern Chile. *J. Volcanol. Geotherm. Res.* **2023**, *439*, 107840. [CrossRef]
65. Naismith, A.K.; Watson, I.M.; Escobar-Wolf, R.; Chigna, G.; Thomas, H.; Coppola, D.; Chun, C. Eruption frequency patterns through time for the current (1999–2018) activity cycle at Volcán de Fuego derived from remote sensing data: Evidence for an accelerating cycle of explosive paroxysms and potential implications of eruptive activity. *J. Volcanol. Geotherm. Res.* **2019**, *371*, 206–219. [CrossRef]
66. Naismith, A.K.; Phillips, J.; Barclay, J.; Armijos, M.T.; Watson, I.M.; Chigna, W.; Chigna, G. Transitions: Comparing timescales of eruption and evacuation at Volcán de Fuego (Guatemala) to understand relationships between hazard evolution and responsive action. *J. Appl. Volcanol.* **2024**, *13*, 1–26. [CrossRef]
67. Di Traglia, F.; Calvari, S.; D'Auria, L.; Nolesini, T.; Bonaccorso, A.; Fornaciai, A.; Esposito, A.; Cristaldi, A.; Favalli, M.; Casagli, N. The 2014 Effusive Eruption at Stromboli: New Insights from In Situ and Remote-Sensing Measurements. *Remote Sens.* **2018**, *10*, 2035. [CrossRef]
68. Zakšek, K.; Hort, M.; Lorenz, E. Satellite and Ground Based Thermal Observation of the 2014 Effusive Eruption at Stromboli Volcano. *Remote Sens.* **2015**, *7*, 17190–17211. [CrossRef]
69. Inguaggiato, S.; Vita, F.; Cangemi, M.; Mazot, A.; Sollami, A.; Calderone, L.; Morici, S.; Paz, M.P.J. Stromboli volcanic activity variations inferred from observations of fluid geochemistry: 16 years of continuous monitoring of soil CO_2 fluxes (2000–2015). *Chem. Geol.* **2017**, *469*, 69–84. [CrossRef]
70. Branney, M.J.; Kokelaar, B.P. Pyroclastic density currents and the sedimentation of ignimbrites. *Geol. Soc. Lond.* **2002**, *27*, 1–143.